Binding Sites for Mg(II) in H^+-ATPase from *Bacillus* PS3 and in the $\alpha_3\beta_3\gamma$ Subcomplex Studied by One-Dimensional ESEEM and Two-Dimensional HYSCORE Spectroscopy of Oxovanadium(IV) Complexes: A Possible Role for β-His-324

Clotilde Buy,[‡] Tadashi Matsui,[§] Sandra Andrianambinintsoa,[‡] Claude Sigalat,[‡] Guy Girault,[‡] and Jean-Luc Zimmermann*,[‡]

Département de Biologie Cellulaire et Moléculaire, Section de Bioénergétique, CEA/Saclay, Bât. 532, F-91191 Gif-sur-Yvette, France, and Research Laboratory of Resources Utilization, Tokyo Institute of Technology, Yokohama 226, Japan

Received July 22, 1996[⊗]

ABSTRACT: The binding sites for Mg^{2+} in wild type F1 ATPase (TF1) and in the $\alpha_3\beta_3\gamma$ subcomplex from the thermophilic bacterium *Bacillus* PS3 have been studied by EPR and by ESEEM and HYSCORE spectroscopy of complexes with the oxovanadium cation VO^{2+}. Complexes of metal-depleted TF1 and substoichiometric amounts of VO^{2+} display low-temperature EPR signals with spectral parameters $g_{\|} = 1.947$ and $g_{\perp} = 1.980$, and hyperfine couplings with ^{51}V, $A_{\|} = 169 \times 10^{-4}$ cm^{-1} and $A_{\perp} = 61 \times 10^{-4}$ cm^{-1}, that are indicative of a binding site for VO^{2+} with nitrogen ligands from the protein. This binding site is probably identical with the metal binding site with strong affinity M1 that has been characterized using Mn^{2+} in a previous study [Buy, C., Girault, G., & Zimmermann, J. L. (1996) *Biochemistry 35*, 9880−9891]. The three-pulse ESEEM spectrum of the VO^{2+} complex with TF1 shows a frequency pattern with spectral properties that are evidence for two nitrogen ligands to the VO^{2+} with hyperfine couplings $A_1 = 4.75$ MHz and $A_2 = 6.5$ MHz and nuclear quadrupole parameters $e^2Qq_1 = 2.8-3.2$ MHz and $e^2Qq_2 = 2.0-2.3$ MHz. The ligands are identified as a lysine terminal amine and a histidine imidazole, which are proposed as Lys-164 and His-324 from a β subunit. The HYSCORE data obtained for the VO·TF1 complex show correlations within each pair of the ESEEM ν_{dq} peaks from the ^{14}N nuclei, confirming the interpretation of the one-dimensional spectra. Evidence for the formation of a ternary complex by addition of VO^{2+} and ATP to metal-depleted TF1 is shown in the EPR and ESEEM spectra and in the contour plots of the HYSCORE data. Two pairs of correlation patterns are resolved in addition to the peaks from the two ^{14}N ligands, which are interpreted as hyperfine couplings with $^{31}P_\beta$ and $^{31}P_\gamma$ of the ATP that binds the VO^{2+} cation. The assignment of the two hyperfine couplings to the specific phosphates, $A(^{31}P_\beta) = 15.5$ MHz and $A(^{31}P_\gamma) = 8.7$ MHz, in the VO·TF1·ATP complex is proposed by comparison with those measured for VO^{2+} in solution with ATP at pH 6.3 and 2.3. These results are discussed in light of the previous data with the analogous Mn·TF1 complex, and a model is proposed in which the native Mg^{2+} in the M1 site is coordinated by the side chain of β-Lys-164 and is in close proximity to a histidine residue (probably β-His-324) that may have a critical role. Additional coordination by two phosphates from ATP (probably the β- and γ-phosphates) is observed in the ternary complex VO·TF1·ATP. ESEEM and HYSCORE data are also obtained for the analogous complexes VO·$\alpha_3\beta_3\gamma$ and VO·$\alpha_3\beta_3\gamma$·ATP that show very similar properties in terms of coordination of the divalent metal cation, except for the lysine ligand that is found to be lost in the ternary complex with ATP. It is suggested that this observation may reflect changes in the metal and nucleotide active sites that are associated with the absence of the δ and ϵ subunits in the subcomplex.

Mg^{2+} cations are essential cofactors in a variety of biological processes, and virtually all enzymes with phosphate cofactors, including adenosine triphosphate (ATP),[1] require Mg^{2+} for their functions. A large and important class of Mg^{2+}-activated enzymes is made up of those catalyzing the transfer of substituted phosphoric acids, and this includes kinases, phosphatases, and synthetases (Heaton, 1990). ATPsynthases of the F type are membrane-bound proteins that catalyze the phosphorylation of ADP to ATP by using a transmembrane proton gradient as a source of energy. Like all synthetases, they require divalent metal cations such as Mg^{2+} for activity. The soluble part F1 of the ATPsynthase enzyme can be isolated and retains the ability to hydrolyze ATP to ADP; it is therefore referred to as an ATPase and

* Author to whom correspondence should be addressed: Fax: +33 (0)1 69 08 87 17. E-mail: zimmermann@dsvidf.cea.fr.

[‡] CEA/Saclay.

[§] Tokyo Institute of Technology.

[⊗] Abstract published in *Advance ACS Abstracts,* November 1, 1996.

[1] Abbreviations: ADP, adenosine 5′-diphosphate; ATP, adenosine 5′-triphosphate; CF1, F1 ATPase from spinach chloroplast; CW, continuous wave; EDTA, ethylenediaminetetraacetic acid; EPR, electron paramagnetic resonance or, equivalently, electron spin resonance or ESR; ESEEM, electron spin echo envelope modulation; FT, Fourier transform; HEPES, *N*-(2-hydroxyethyl)piperazine-*N*′-2-ethanesulfonic acid; HPLC, high-performance liquid chromatography; HYSCORE, hyperfine sublevel correlation spectroscopy; MF1, F1 from bovine heart mitochondria; NQR, nuclear quadrupole resonance; OGP, *n*-octyl β-D-glucopyranoside; TF1, F1 from thermophilic *Bacillus* PS3; TRIS, 2-amino-2-(hydroxymethyl)propane-1,3-diol.

S0006-2960(96)01811-9 CCC: $12.00

contains the active binding sites for nucleotides. The F1 ATPase also bears the sites for divalent metal binding, and characterization of binding sites for Mn^{2+} or VO^{2+} has been reported for the ATPases isolated from spinach chloroplasts (CF1) and from the thermophilic bacterium *Bacillus* PS3 (TF1) (Houseman et al., 1994a,b, 1995; Buy et al., 1996).

TF1 is made of five different subunits with a stoichiometry of $\alpha_3\beta_3\gamma\delta\epsilon$; it is highly homologous with CF1, the enzyme from chloroplasts for which six binding sites for divalent metal cations have been determined (Hiller & Carmeli, 1985). The three sites with the highest affinity for Mn^{2+} are known as the M1−M3 metal binding sites, and it has been reported by EPR and ESEEM using VO^{2+} as a paramagnetic probe that both sites M2 and M3 probably involve, in the absence of nucleotide, one amine ligand each from a lysine side chain (Houseman et al., 1994a). The lysine ligands were found axial to the VO^{2+} cation and were identified as α-Lys-175 and β-Lys-162, respectively (Houseman et al., 1995), as judged from the amino acid sequence and the crystal structure of the mitochondrial F1 (Abrahams et al., 1994). In addition, Houseman et al. (1995) established a correlation between the identified metal sites M2 and M3 and two of the six binding sites for nucleotides that have been found in the α and β subunits of CF1 (Cross, 1988; Girault et al., 1988).

A nucleotide binding site with a very high affinity, N1, has been identified in CF1 that contains a bound ADP molecule which is difficult to deplete (Bruist & Hammes, 1981). Interaction of this N1 site with Mn^{2+} bound to the metal binding site with highest-affinity M1 was recently demonstrated by EPR and ESEEM spectroscopy (Buy et al., 1996). The measured hyperfine coupling with ^{31}P was evidence for binding of the Mn^{2+} by the β-phosphate of the bound ADP. Rather interestingly, TF1, by contrast with CF1, can be isolated with no bound ADP, and nucleotide binding to Mn^{2+} in the M1 site was found only after addition of exogenous ATP (Buy et al., 1996).

Interaction between Mn^{2+} and nucleotide bound to CF1 and TF1 could be demonstrated through the detection of the typical hyperfine couplings with ^{31}P from nucleotides bound to Mn^{2+}. This is all the more interesting because significant changes in these hyperfine couplings that followed the addition of ATP were measured, which could actually reflect conformational changes in the nucleotide site. These measurements were made possible through the use of ESEEM spectroscopy which is a high-resolution technique based on the pulsed EPR method (Kevan, 1990). One-dimensional ESEEM spectroscopy is well-suited for the detection of small couplings with nuclei in the neighborhood of the paramagnetic species. For Mn^{2+} binding sites in enzymes, hyperfine couplings with ^{2}H, ^{14}N, ^{17}O, and ^{31}P from ligands of the divalent metal cation have been detected. Thus, in addition to the interaction with ^{31}P from phosphate-derived ligands, ligands to the Mn^{2+} center with ^{14}N donors like histidine or lysine can be identified (Espe et al., 1995; Buy et al., 1996, and references therein).

Not only is the Mn^{2+} cation a particularly useful spectroscopic probe for studying the structural properties of Mg^{2+} sites in proteins, and in particular the M1 site of CF1 and TF1, but it is also usually a highly efficient divalent metal cofactor for the enzyme. In fact, the ATPase activities of CF1 and TF1 with Mg^{2+} and Mn^{2+} are comparable, and this would probably allow spectroscopic studies of catalytic intermediates with bound Mn^{2+}. The high spin multiplicity of the Mn^{2+} cation ($S = {}^5/_2$) may, however, be a disadvantage for the ESEEM studies because magnetic couplings with the five fine structure transitions may contribute to the frequency pattern in the ESEEM, with a resulting coupling scheme of increased complexity (Larsen et al., 1993). This precludes a detailed analysis of the spectra of Mn^{2+} with ligands with ^{14}N for which the hyperfine coupling A and the quadrupole coupling e^2qQ cannot be readily determined from the ESEEM patterns and for which only a qualitative interpretation is presently available.

As mentioned above, the structures of the M2 and M3 metal binding sites of CF1 have been probed using VO^{2+} as a paramagnetic substitute for Mg^{2+} (Houseman et al., 1994a,b, 1995). Although VO^{2+} may not functionally replace Mg^{2+} with the same efficiency as Mn^{2+} for the ATPase activity of CF1 and TF1, the CW EPR spectral properties of complexes with VO^{2+} are of special interest because the set of equatorial ligands can be empirically inferred from the values of the hyperfine couplings with ^{51}V that produce well-resolved lines in spectra at X-band. In fact, the EPR spectral parameters, as well as the ligand hyperfine couplings measured by ENDOR and ESEEM spectroscopy of the VO^{2+} cation used as a substitute for Mg^{2+}, have been successfully used to study the divalent metal binding sites in a variety of enzymes (Chasteen, 1981; Eaton & Eaton, 1990).

In the present work, a detailed spectroscopic study of a metal site (probably the M1 site) in TF1 and in the $\alpha_3\beta_3\gamma$ subcomplex with bound VO^{2+} is presented, which includes simulation of the CW EPR spectra, analysis of the ESEEM frequency patterns, and comparison with those of VO^{2+} sites with known ligands. In addition, a characterization of this VO^{2+} site by HYSCORE spectroscopy, which is a two-dimensional version of ESEEM, is reported, allowing the assignments of the ESEEM frequencies in the binary VO·TF1 complex to two different nitrogen ligands. For the ternary complex with TF1, VO^{2+}, and ATP, the HYSCORE correlation patterns are evidence for binding of the VO^{2+} cation to both TF1 and ATP, and the hyperfine coupling parameters with ^{31}P from ATP (probably $^{31}P_\beta$ and $^{31}P_\gamma$) are reported. A similar study with the $\alpha_3\beta_3\gamma$ subcomplex of TF1 shows very similar spectroscopic properties in terms of the metal binding site with the strongest affinity. Coordination changes at the VO^{2+} site in the $\alpha_3\beta_3\gamma$ complex in the presence of ATP are observed, a behavior that appears to be different from that in TF1. A model for the M1 binding site in the presence of VO^{2+} is presented on the basis of these results.

MATERIALS AND METHODS

The soluble part of the ATPase/synthase extracted from *Bacillus* PS3 (TF1) was prepared from cell paste as described previously (Buy et al., 1996). Purified TF1 was stored at 4 °C as a precipitate in ammonium sulfate at 50% saturation. Before preparation of the protein samples with VO^{2+}, the protein precipitates were dialyzed for 24 h in 50 mM HEPES−NaOH and 10 mM EDTA at pH 8. This was followed by a 48 h dialysis in 50 mM HEPES−NaOH at pH 8 and by a 3 h dialysis in the same buffer at pH 7. The protein was then concentrated to ≥30 mg/mL, and protein concentrations were determined as described previously (Buy et al., 1996). The molecular mass of TF1 was taken as

385 350 Da, according to the molecular masses of the different subunits published by Ohta et al. (1988). VO^{2+} or VO^{2+} and ATP were added to the EPR samples from a freshly prepared solution in 200 mM maleate at pH 6.3 that was previously bubbled with dry nitrogen to remove dissolved oxygen. The addition was performed with vigorous stirring. The EPR samples were then frozen within 2 min in liquid nitrogen where they were stored until use.

The overexpression of the α, β, and γ subunits of TF1 in *Escherichia coli* was performed by using the expression plasmids of the $\alpha_3\beta_3\gamma$ complex, and the obtained complex was purified as described previously (Matsui & Yoshida, 1995) in the laboratory of Prof. Yoshida. For the preparation of the EPR samples, the lyophilized $\alpha_3\beta_3\gamma$ complex was weighed and was then supplemented with 50 mM HEPES−NaOH at pH 7. The concentration was verified by the Bradford technique, as above, and showed very good correspondence with that deduced from the mass of the complex and the volume of buffer added to it. The addition of VO^{2+} and storage of the EPR samples were performed as described above. The molecular mass of $\alpha_3\beta_3\gamma$ was taken as 351 360 Da (Ohta et al., 1988).

The Mg^{2+} contents of TF1 and the $\alpha_3\beta_3\gamma$ complex were determined by atomic absorption spectroscopy as previously described (Buy et al., 1996).

The concentration of nucleotides and the catalytic activity of the samples of TF1 and $\alpha_3\beta_3\gamma$ were determined using HPLC as described previously (Buy et al., 1996) with the following modifications. The ATPase activity was measured at 37 °C in a Tris-SO_4 buffer at pH 8, with 180 μM $MgSO_4$ (or $MnSO_4$ or $VOSO_4$, depending of the metal cofactor tested) and 1 mM ATP. In some samples, 25 mM OGP (*n*-octyl β-D-glucopyranoside) was added as a potential activator of the catalytic activity.

Frozen solutions of VO^{2+} with different ligands (imidazole, glycine, HEPES, ATP, or ADP) were obtained as follows. For VO^{2+} complexed with imidazole, VO^{2+} (1.56 mM) was added from a stock solution of 78.2 mM $VOSO_4$ at pH 2 [concentration determined using $\epsilon_{750} = 18$ M^{-1} cm^{-1} (Chasteen, 1981)] to a degassed solution of 200 mM imidazole. The final pH was 8.7, and ethanol (25% volume) was added to the sample. VO^{2+} complexed with glycine was prepared in the same way, except that the final pH was adjusted to 8.5 with NaOH. For VO^{2+} with HEPES, 25 μL of a 7.82 mM $VOSO_4$ solution in 200 mM maleate buffer at pH 6.3 was added to 1 mL of 50 mM HEPES at pH 7. The EPR sample of VO^{2+} complexed with ATP was prepared as follows. VO^{2+} was added from the stock solution at pH 2 to a degassed solution of 24.5 mM ATP in 200 mM maleate at pH 6.3 (final concentration of $VOSO_4 = 7.82$ mM), and 20% ethanol was added to the sample. For VO^{2+} complexed with ADP, the procedure was similar to that for ATP. All the samples were frozen to a liquid nitrogen temperature within 3 min after they were made.

EPR spectra at X-band were recorded with a Bruker 200D spectrometer using a standard rectangular TE_{102} cavity. The spectrometer was equipped with a microwave frequency counter (Hewlett-Packard 5350B) and an NMR gaussmeter (Bruker ER035M). A sample temperature of 4.2 K was achieved using a liquid helium cryostat (Oxford Instruments). The simulations of the EPR spectra were performed using perturbation theory as described previously (Bonvoisin et al., 1992).

For the quantitation of VO^{2+} in the EPR samples containing TF1 or $\alpha_3\beta_3\gamma$, the X-band EPR spectra of a series of samples of $VOSO_4$ in different concentrations in 200 mM degassed maleic acid at pH 6.7 were recorded under the same experimental conditions as for the biological samples ($T =$ 4.2 K, $P = 2$ mW). The sum of the areas under the $-7/2_{||}$ and $-5/2_{||}$ features in the derivative EPR signal was plotted as a function of the concentration of VO^{2+}, leading to a linear dependance ($R = 0.98$ for the linear regression). The actual concentration of VO^{2+} in the TF1 and $\alpha_3\beta_3\gamma$ samples and the VO^{2+}/protein ratio (or complex) were then deduced from these measurements.

One- and two-dimensional ESEEM experiments were performed at 4.2 K with a Bruker ER 380 pulsed EPR spectrometer equipped with an Oxford Instruments liquid helium immersion dewar. The one-dimensional experiments (three-pulse ESEEM) were performed using the microwave pulse sequence $\pi/2-\tau-\pi/2-T-\pi/2$ that produces a stimulated echo at time τ after the last pulse (Kevan, 1990). The length of the pulses was 16 ns. The amplitude of the stimulated echo was recorded as a function of the interpulse time T, and the modulation functions convoluted with the overall decay function of the echo (ESEEM) were Fourier transformed as described previously (Buy et al., 1996). Experimentally, it is necessary to use a four-step phase cycling $(0, 0, 0)-(0, \pi, 0)-(\pi, 0, 0)+(\pi, \pi, 0)$ algorithm to eliminate the contributions from secondary echoes to the stimulated echo envelope (Fauth et al., 1986). The τ values were taken as twice the inverse of the proton Larmor frequency to minimize the modulations from the weakly coupled protons in the stimulated echo signal (Mims & Peisach, 1981). Two-dimensional ESEEM experiments were based on the HYSCORE experiment with a sequence of four microwave pulses $\pi/2-\tau-\pi/2-t_1-\pi-t_2-\pi/2$ that produces an inverted echo at time τ after the last pulse (Höfer et al., 1986). This sequence can be divided into four domains: preparation (time τ), evolution (time t_1), mixing (π pulse), and detection (time t_2). The mixing π pulse creates correlations between those ESEEM frequencies that correspond to nuclear transitions of the same nuclei (Höfer et al., 1986; Shane et al., 1992). Contour plots of the data after Fourier transformation in both time domains t_1 and t_2, referred to as f_1 and f_2 directions, may reveal pairs of peaks that are symmetrically positioned on each side of the diagonals in the positive (f_2, f_1) and/or negative (f_2, $-f_1$) quadrants. In addition to having the potential for separating complex patterns of frequency lines that overlap in the one-dimensional ESEEM spectra, the two-dimensional HYSCORE plots may be of valuable significance for the assignments of the ESEEM peaks in terms of nuclear transitions (Höfer et al., 1986; Shane et al., 1992). In the experiments reported in the present study, the length of the mixing π pulse was adjusted in order to have the maximum inversion of the stimulated echo (Höfer, 1991). Spectra with different τ values were recorded for the same sample in an attempt to minimize suppression effects due to the choice of τ (Höfer, 1994). A four-step phase cycle $(0, 0, 0, 0)-(0, 0, 0, \pi)+(0, 0, \pi, 0)-(0, 0, \pi, \pi)$ was used to remove unwanted echoes (Gemperle et al., 1990). The measured signal was then treated as follows. The unmodulated relaxation decay was eliminated by subtracting a suitable background correction in both directions; Hamming apodization and zero filling to 2^9 points were performed in both

Table 1: ATPase Activity [μmol of ADP·min^{-1}·(mg of protein)$^{-1}$] of TF1 and $\alpha_3\beta_3\gamma$

metal cofactor and presence or absence of OGP[a]	TF1	$\alpha_3\beta_3\gamma$
Mg^{2+}	20.5	6.5
Mg^{2+} and OGP	19.8	6.4
Mn^{2+}	23.9	5.6
Mn^{2+} and OGP	15.4	4.8
VO^{2+}	0.5	0.7
VO^{2+} and OGP	2.6	0.6

[a] See Materials and Methods.

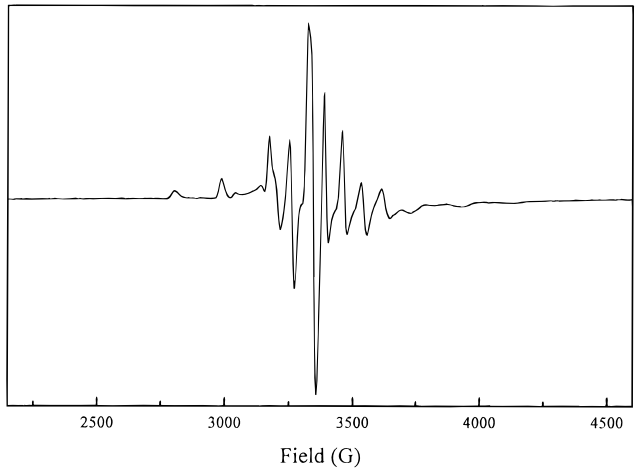

FIGURE 1: X-Band EPR spectrum of a sample containing metal-depleted TF1 and supplemented with exogenous VO^{2+} (0.9 VO^{2+}/TF1). Experimental conditions were the following: temperature, 4.4 K; microwave power, 0.2 mW; microwave frequency, 9.435 GHz; and modulation amplitude, 9.65 G.

dimensions, and f_2 and f_1 Fourier transform were then performed, using the WinEPR software from Bruker.

RESULTS

TF1 isolated without any nucleotide and depleted of divalent metal cations by incubation with ammonium sulfate and dialysis with EDTA contains virtually no metal bound to the M1−M3 binding sites (Buy et al., 1996). The ATPase activity of metal-depleted TF1 was measured to test the relative efficiency of Mg^{2+}, Mn^{2+}, and VO^{2+} ions acting as cofactors of the hydrolysis reaction. In fact, Mn^{2+} is a very efficient substitute for Mg^{2+} both in the presence and in the absence of OGP (Table 1), confirming the earlier observations (Buy et al., 1996). The activity in the presence of VO^{2+} is significantly reduced, however, being approximately 2.5−10% of that with Mg^{2+}. This may contradict the earlier data by Houseman et al. (1994a), who reported that VO^{2+} can substitute for Mg^{2+} as a cofactor for ATPase activity catalyzed by CF1, the enzyme from chloroplasts. Additional information relevant to this question will be given below. Supplementing a sample of TF1 with VO^{2+} in a ratio of 0.9/1 will probably fill the strongest-affinity metal binding site M1 in a manner similar to what has been described with Mn^{2+} (Buy et al., 1996). The CW EPR spectrum of VO^{2+} bound to TF1 in the M1 site is shown in Figure 1. This spectrum exhibits 16 lines arising from the coupling of the unpaired electron spin ($S = {}^1/_2$) of the VO^{2+} ion with the ^{51}V nucleus ($I = {}^7/_2$) with an axial hyperfine coupling tensor (Chasteen, 1981). The eight smaller and widely spaced lines are roughly separated by $A_{||}$, and the eight more intense lines are separated by $A_\perp$. The EPR parameters used in the simulation that best fit the spectrum of Figure 1 ($g_{||} = 1.947$, $g_\perp = 1.980$, and $A_{||} = 169 \times 10^{-4}$ cm^{-1}, and $A_\perp = 61 \times 10^{-4}$ cm^{-1}) are different from those for VO^{2+} in H_2O or in maleate or HEPES buffer (Table 2) and are evidence of binding of the added VO^{2+} ions to the TF1 protein. In addition, the time between preparation of the EPR sample with TF1 and freezing in liquid N_2 was long enough to allow precipitation of free VO^{2+}, probably as $VO(OH)_2$, which is EPR silent (Chasteen, 1981). In fact, an EPR sample prepared in the same manner but without TF1 gave no detectable EPR signal (not shown). This latter observation is quite in line with that of Chasteen (1981), who reports that, at pH 7 and in the absence of any chelating agent, the VO^{2+} concentration in the buffer is too low to be detected. Thus, only VO^{2+} bound to the protein can be detected by EPR. Also, an EPR spectrum similar to that shown in Figure 1 for TF1 has been reported for VO^{2+} bound to the M2 and M3 metal binding sites of CF1 (Houseman et al., 1994a,b, 1995). A sample containing the $\alpha_3\beta_3\gamma$ complex and VO^{2+} (ratio of 0.4 $VO^{2+}/\alpha_3\beta_3\gamma$) was also studied by EPR, and the EPR parameters of the spectrum were close to those obtained for TF1 ($g_{||} = 1.950$, $g_\perp = 1.980$, $A_{||} = 165 \times 10^{-4}$ cm^{-1}, and $A_\perp = 56.5 \times 10^{-4}$ cm^{-1}) (Table 2). Because it was verified that the $\alpha_3\beta_3\gamma$ complex contained virtually no Mg^{2+} (0.15 ± 0.02 $Mg^{2+}/\alpha_3\beta_3\gamma$) and no nucleotide ($\leq 0.01$ ADP/$\alpha_3\beta_3\gamma$), these data suggest that VO^{2+} binds to a metal site that is probably analogous to the M1 site in TF1. The CW EPR spectra were also compared with those obtained for VO^{2+} bound with glycinate and imidazole, as well as those for VO^{2+} in H_2O and VO^{2+} with the two buffers used during the preparation of the protein samples (maleate and HEPES). All of them display the typical 16-line spectrum described above (not shown). The EPR parameters obtained from the simulation of these spectra are listed in Table 2. The parameters, especially $A_{||}$ and $A_\perp$, calculated for VO^{2+} in water, with imidazole or with glycinate, are in line with published data [Mulks et al., 1982; see also Houseman et al. (1994a)], although the slightly different value for $A_{||}$ (160×10^{-4} cm^{-1}) found here for VO^{2+} with glycinate may originate from differences in sample preparation. The amplitude of $A_{||}$ for the VO^{2+} cation in a specific site has been shown to depend on the nature of the equatorial ligands, and in a specific environment, it can be related to the hyperfine coupling with each ligand independently by an additivity relationship (Chasteen, 1981). However, more than one combination of ligands can fulfill the

Table 2: ^{51}V Hyperfine Couplings and **g** Tensors for VO^{2+} Complexes Measured from the EPR Data

complexing ligand(s)	$A_\perp$ ($\times 10^{-4}$ cm^{-1})	$A_{||}$ ($\times 10^{-4}$ cm^{-1})	$g_\perp$	$g_{||}$
TF1 (0.9 VO^{2+}/TF1)	61.0	169.0	1.980	1.947
ATP and TF1 (0.93 VO^{2+}/TF1 and 3 ATP/VO^{2+})	64.0	178.0	1.980	1.935
$\alpha_3\beta_3\gamma$ (0.4 $VO^{2+}/\alpha_3\beta_3\gamma$)	56.5	165.0	1.980	1.950
ATP and $\alpha_3\beta_3\gamma$ (1.4 $VO^{2+}/\alpha_3\beta_3\gamma$ and 3 ATP/VO^{2+})	67.0	180.0	1.980	1.935
H_2O	72.0	182.5	1.980	1.935
HEPES (pH 6.3)	63.0	172.0	1.979	1.940
maleate (pH 6.7)	63.0	172.0	1.979	1.940
ATP in maleate (pH 6.3)	65.0	178.0	1.980	1.935
glycine	54.5	160.0	1.981	1.956
imidazole	57.2	162.0	1.980	1.952

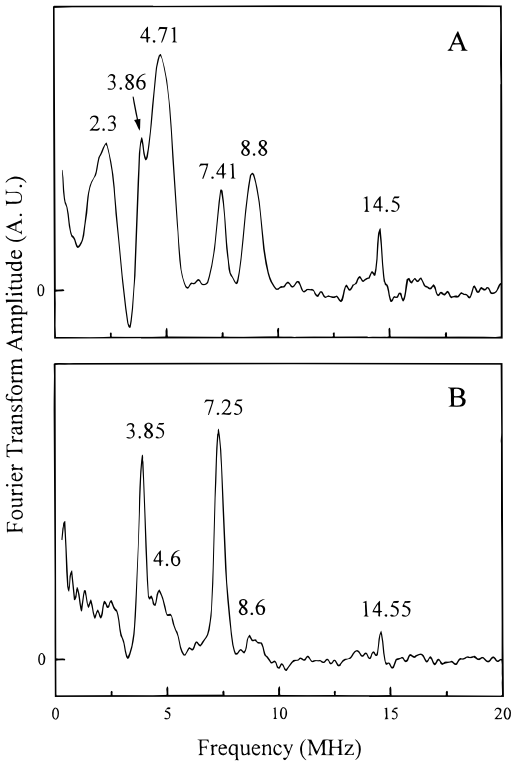

FIGURE 2: Three-pulse FT ESEEM spectra of VO^{2+} bound to TF1 (0.9 VO^{2+}/TF1) (A) and VO^{2+} bound to $\alpha_3\beta_3\gamma$ (0.4 $VO^{2+}/\alpha_3\beta_3\gamma$) (B). The data were obtained at a temperature of 4.2 K, a microwave frequency of 9.59 GHz, and a magnetic field setting of 3427 G. The interpulse time τ was 136 ns, and the time interval between successive spin echo pulse sets was 30.7 ms.

same additivity relationship, and it is not always possible to ascertain the full coordination sphere of VO^{2+} in an unknown site. Nevertheless, a qualitative comparison between different hyperfine coupling parameters can help in finding some possible ligands of the VO^{2+}. The reduced $A_{||}$ values observed for VO^{2+} bound to TF1 or the $\alpha_3\beta_3\gamma$ complex could reflect coordination by one or more nitrogen donors; in fact, a lysine has been reported as a possible ligand of Mn^{2+} in the M1 site of TF1 (Buy et al., 1996), and similar observations have been made for the CF1 metal binding sites where it was proposed that the terminal amine of a lysine residue was a ligand of the VO^{2+} in the M2 site (Houseman et al., 1994a). When TF1 depleted of nucleotide and Mg^{2+} is supplemented with VO^{2+} and ATP (3 ATP/TF1) in a ratio of 0.93 VO^{2+}/protein, the VO^{2+} site is characterized by an EPR spectrum that can be simulated with hyperfine coupling parameters ($A_{||} = 178 \times 10^{-4}$ cm^{-1}) that are close to those of VO^{2+} with ATP (Table 2), suggesting that VO^{2+} also binds to ATP, perhaps in the ternary complex VO·TF1·ATP.

ESEEM has proven to be a very powerful technique for studying the environment of metal sites in proteins with bound VO^{2+} [see Chasteen (1981) and Eaton and Eaton (1990) for reviews]. Recently, ESEEM data for VO^{2+} complexes with CF1 have been reported, and a model for binding sites M2 and M3 was proposed (Houseman et al., 1994a, 1995). Figure 2A displays the Fourier transform of the three-pulse ESEEM signal of VO^{2+} bound to TF1 in the M1 site. The signal was recorded at 3427 G, a magnetic field that corresponds to the central line of the VO^{2+} EPR spectrum, i.e. the $M_I = -1/2_{||}$ transition, with some contributions from the $M_I = -1/2_{\perp}$ transition. Five major and well-resolved nuclear frequencies at 2.3, 3.86, 4.71, 7.41, and 8.8 MHz are identified in the spectrum. The smaller peak at ≈14.5 MHz originates from the hyperfine interactions of VO^{2+} with weakly coupled protons and is almost suppressed due to the choice of τ. Figure 2B shows that the $\alpha_3\beta_3\gamma$ complex with VO^{2+} displays an ESEEM spectrum with very similar frequencies at 2.4, 3.85, 4.6, 7.25, and 8.6 MHz (and the proton frequency at 14.5 MHz), although the peaks at 4.6 and 8.6 MHz appear weaker than in the TF1 sample. The spectrum for control samples prepared with VO^{2+} in HEPES buffer had no modulation frequency at all (not shown), confirming that the frequencies described above in the TF1 and the $\alpha_3\beta_3\gamma$ complex are due to interactions of VO^{2+} with the protein and the complex, respectively, and not with the buffer.

In the three-pulse ESEEM spectra obtained for samples with VO^{2+} in solution with glycinate, nuclear frequencies are observed at ≈3.8 and 7.45 MHz; for VO^{2+} with imidazole, ESEEM frequencies are resolved at ≈4.8 and 8.9 MHz (not shown). Both spectra were recorded at the EPR absorption maximum H of 3450 G, as for the samples with VO^{2+} bound to the protein or the $\alpha_3\beta_3\gamma$ complex. These results are well in line with those published by Tipton et al. (1989) for VO^{2+} complexes with glycinate and imidazole. The pair of frequencies in the glycinate or imidazole spectrum is assigned to the two double-quantum transitions from ^{14}N nuclei bound to the VO^{2+} cation. The ESEEM frequencies observed for the biological samples are close to those for the glycinate and imidazole samples. A magnetic interaction between VO^{2+} and two different coordinating ^{14}N nuclei may give rise to two double-quantum transition pairs at 3.86 and 7.41 MHz (3.85 and 7.25 MHz for the $\alpha_3\beta_3\gamma$ complex) due to a first ^{14}N atom [hereafter referred to ^{14}N-(1)] and at 4.71 and 8.8 MHz (4.6 and 8.6 MHz for the $\alpha_3\beta_3\gamma$ complex) due to a second atom $^{14}N(2)$. This interpretation is supported by the magnetic field dependence of the ESEEM frequencies. For nuclei with $I = 1$, if the anisotropic hyperfine interaction is very small compared with the isotropic hyperfine and quadrupole interactions (Flanagan & Singel, 1987, 1988; Cosgrove & Singel, 1990), then the double-quantum frequencies $\nu_{dq\pm}$ are given by (Astashkin et al., 1985; Flanagan & Singel, 1987)

$$\nu_{dq\pm} = 2[(\nu_L \mp A_{iso}/2)^2 + K^2(3 + \eta^2)]^{1/2} \qquad (1)$$

where $K = e^2qQ/4$ and η are the quadrupole coupling constant and the asymmetry parameter, respectively, A_{iso} is the isotropic hyperfine coupling constant, and ν_L is the Larmor frequency at the measuring magnetic field. This expression can be rewritten as

$$\nu_{dq\pm}{}^2/4 - \nu_L{}^2 = \mp A_{iso}\nu_L + A_{iso}{}^2/4 + K^2(3 + \eta^2) \quad (2)$$

In order to test the assignment made above of the peaks in the TF1 and $\alpha_3\beta_3\gamma$ spectra to double transitions of coupled ^{14}N, we have plotted the frequencies of the ESEEM peaks obtained for magnetic field settings ranging from ≈2800 to ≈4200 G, corresponding to the limits of the VO^{2+} EPR absorption line at X-band, as $\nu_{dq\pm}{}^2/4 - \nu_L{}^2$ as a function of $-\zeta_\pm\nu_L$, where the sign variable $\zeta_\pm$ refers to the sign of M_S in the manifold associated with $\nu_{dq\pm}$. Figure 3 shows plots for the pairs of peaks obtained for the different samples. The linear relationship between $\nu_{dq\pm}{}^2/4 - \nu_L{}^2$ and $-\zeta_\pm\nu_L$ is quite obvious from linear regressions of the data points corre-

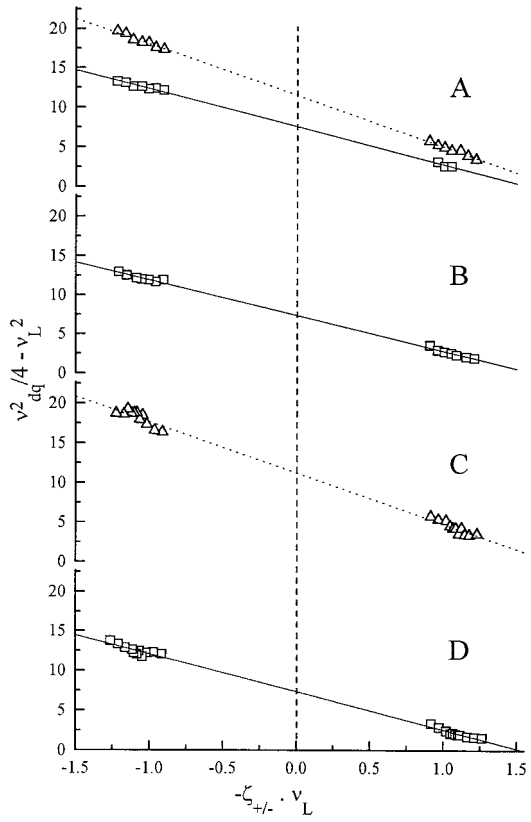

FIGURE 3: Plots of $\nu_{dq}^2/4 - \nu_L^2$ as a function of $-\zeta_\pm\nu_L$ for the ESEEM peaks in spectra of VO^{2+} complexes: TF1 (0.9 VO^{2+}/TF1) (A), $\alpha_3\beta_3\gamma$ (0.4 $VO^{2+}/\alpha_3\beta_3\gamma$) (B), imidazole (C), and glycine (D). ν_{dq} is a double-quantum frequency of the ^{14}N coordinating the VO^{2+}; ν_L is the Larmor frequency of ^{14}N, and $\zeta_\pm$ is the sign of the $M_S = \pm^1/_2$ in the manifold associated with ν_{dq}.

Table 3: Hyperfine Coupling A_{iso} and Nuclear Quadrupole Coupling e^2qQ of ^{14}N Bound to VO^{2+} Measured from the ESEEM Data

complexing ligand	A_{iso} (MHz)	$K^2(3+\eta^2)$ (MHz^2)	e^2qQ (MHz) lower limit[a]	e^2qQ (MHz) upper limit[a]	assignment
glycine	4.8	1.73	2.63	3.03	
imidazole	6.4	0.99	1.99	2.30	
TF1	4.75	1.95	2.80	3.22	lysine
(0.9 VO^{2+}/TF1)	6.5	1.03	2.03	2.34	histidine
$\alpha_3\beta_3\gamma$	4.53	2.27	3.01	3.48	lysine
(0.4 $VO^{2+}/\alpha_3\beta_3\gamma$)					

[a] The lower and upper limits for e^2qQ were estimated from the values of $K^2(3+\eta^2)$ with $0 \le \eta \le 1$. $K^2(3+\eta^2)$ was calculated from the ESEEM data (see text), and $e^2qQ = 4K$.

sponding to each pair of peaks (Figure 3), except perhaps for the frequency peaks at ≈4.6 and ≈8.6 MHz in Figure 2B for the spectrum of the $\alpha_3\beta_3\gamma$ complex, for which a relatively low intensity precluded any further analysis. This is taken as evidence that the four ESEEM peaks in the TF1 and $\alpha_3\beta_3\gamma$ samples are double-quantum transitions of two ^{14}N nuclei coupled to the VO^{2+} cation. The hyperfine coupling constant and the parameter $K^2(3+\eta^2)$ were then evaluated using eq 2, and the results are listed in Table 3. We note immediately that all the A_{iso} values calculated here are in the range of 4.5−6.5 MHz, and this is indicative of two coordinating ^{14}N in the biological samples (Eaton et al., 1989; Tipton et al., 1989; Zhang et al., 1993; Dikanov et al., 1995a). On the other hand, the exact cancellation condition requires that $A_{iso}/2 \approx \nu_L$ (Flanagan & Singel, 1987), and this situation occurs for ν_L ranging from 2.25 to 3.25 MHz, depending on the hyperfine coupling. This would correspond to applied magnetic fields of 7300−10560 G, which are well above the limits of the CW EPR spectra that are obtained at X-band for VO^{2+}. In addition, judging from the magnetic parameters listed in Table 3, $A_{iso} - 2\nu_n > 2K$ for all the samples. This in turn indicates that the condition $A_{iso} - 2\nu_n > {}^4/_3K$ mentioned by Flanagan and Singel (1987) for large deviation from exact cancellation is always fulfilled for the samples studied here. In addition, the observation of only the double-quantum peaks of the ^{14}N nuclei being resolved in Figure 2A,B is fully consistent with such large deviation from the exact cancellation condition.

The hyperfine coupling constant $A_{iso} = 4.8$ MHz calculated for the bonded ^{14}N in VO^{2+} with glycinate is in line with the value $A_{iso} = 5.0$ MHz reported by Tipton et al. (1989). The estimated $K^2(3+\eta^2) = 1.73$ MHz^2 corresponds to a range[2] for e^2qQ of 2.6−3.0 MHz for the deprotonated amine nitrogen of glycinate bound to VO^{2+}. Lucken (1969) has found $e^2qQ = 3.99$ MHz for the amine nitrogen in aminomethane. This value is expected to decrease significantly upon coordination of the ^{14}N to the metal [see Ashby et al. (1978)]. The result reported in the present study is consistent with this observation as well as with the value of e^2qQ of 2.55 MHz reported by Tipton et al. (1989). For the imino nitrogen of imidazole bound to VO^{2+}, Table 3 yields $K^2(3+\eta^2) = 0.99$ MHz^2, corresponding to a range[2] for e^2qQ of 1.99−2.3 MHz. This is also consistent with the data from NQR spectroscopy reported for Zn^{2+} and Cd^{2+} complexes with imidazoles ($e^2qQ = 1.93-2.82$ MHz; Ashby et al., 1978). The result from the ESEEM data is also consistent with the value for e^2qQ of 1.6 MHz calculated from ENDOR spectra by Mulks et al. (1982) for imidazole bound to VO^{2+}. Finally, these authors also found $A_z = 6.64$ MHz for the coupling with the bonded nitrogen in $VO(ImH)_4^{2+}$, which is very close to the value extracted here from the ESEEM data, $A_{iso} = 6.4$ MHz (Table 3).

The smaller $^{14}N(1)$ hyperfine couplings, $A_{iso(1)} = 4.75$ MHz and $A_{iso(1)} = 4.53$ MHz, observed in TF1 with 0.9 VO^{2+}/TF1 and in the $\alpha_3\beta_3\gamma$ complex with 0.4 $VO^{2+}/\alpha_3\beta_3\gamma$ are very close to the A_{iso} calculated for VO^{2+} with glycinate (Table 3). According to the hyperfine couplings with ^{14}N that have been reported for metal sites in proteins with VO^{2+}, A_{iso} ranges from 4.3 to 5.2 MHz for coordination of VO^{2+} with the amine ^{14}N of a lysine residue (Tipton et al., 1989; Zhang et al., 1993; Houseman et al., 1994a; Fukui et al., 1995). The estimated A_{iso} values for the $^{14}N(1)$ in the M1 site of TF1 and $\alpha_3\beta_3\gamma$ are also of a similar magnitude, suggesting that the detected $^{14}N(1)$ may be the amine nitrogen of a lysine residue. Finally, we have suggested in a recent EPR and ESEEM study of TF1 that exogenous Mn^{2+} bound to the M1 site was coordinated by a lysine (Buy et al., 1996). The present results are also indicative of a lysine ligand for VO^{2+} in the M1 site.

For the second nitrogen $^{14}N(2)$ detected in the ESEEM spectra of VO^{2+} bound to the M1 site of TF1, $A_{iso(2)} = 6.5$ MHz (Table 3), a value which is close to the A_{iso} of imidazole. The hyperfine coupling between VO^{2+} and the imino ^{14}N of an imidazole ring has been determined in a

[2] The distribution in e^2qQ results from the uncertainty in the asymmetry parameter η and is given for the whole range of the latter, $0 \le \eta \le 1$.

number of compounds or protein complexes with VO^{2+} (Eaton et al., 1989; Gerfen et al., 1991; Reijerse et al., 1991; Dikanov et al., 1995a). In fact, all the reported A_{iso} values range between 6.0 and 7.6 MHz, and in the protein studies, a hyperfine coupling with ^{14}N of this magnitude was taken as evidence of equatorial coordination of VO^{2+} by a histidine imidazole (Eaton et al., 1989; Gerfen et al., 1991; Dikanov et al., 1995a). Thus, $^{14}N(2)$ probably belongs also to the imidazole ring of a histidine residue. Additional evidence for a histidine assignment for the second coupled nitrogen is given by the comparison of the quadrupole parameters. $K^2(3 + \eta^2) = 1.03$ MHz^2 for the $^{14}N(2)$ in TF1, a value which is very close to $K^2(3 + \eta^2) = 0.99$ MHz^2 calculated for the bonded ^{14}N in the VO^{2+} complex with imidazole (Table 3). This corresponds to $e^2qQ = 2.03-2.34$ MHz, a range that is totally consistent with published data for protein and VO^{2+} compounds, for which e^2qQ ranges from 1.52 to 2.0 MHz (Mulks et al., 1982; Gerfen et al., 1991; Fukui et al., 1993).

To strengthen the assignments made above for the frequencies observed in the three-pulse ESEEM spectra for VO^{2+} in TF1 and the $\alpha_3\beta_3\gamma$ complex, two-dimensional ESEEM experiments were performed in an attempt to potentially detect correlation patterns between the frequency peaks. The two-dimensional HYSCORE technique utilizes a four-pulse sequence (Höfer et al., 1986) that includes an inverting π pulse used to correlate the different sublevel transitions belonging to the same electron spin. In the case of VO^{2+} with $S = {}^1/_2$, correlations may be detected between nuclear transitions associated with the two M_S manifolds. As mentioned above, the nuclear frequencies detected in the three-pulse ESEEM experiment and that are connected in the HYSCORE data are associated with the same electron spin, and this can be used to distinguish between hyperfine lines that may overlap in the one-dimensional spectrum (Höfer et al., 1986; Reijerse et al., 1991). Figure 4 shows the contour plot of the Fourier transform in both f_1 and f_2 directions of the HYSCORE data obtained for the sample with VO^{2+} bound to TF1 in the M1 site (0.9 VO^{2+}/TF1). The on-diagonal features in both quadrants are probably due to an incomplete inversion of the π pulse (Gemperle et al., 1990; Höfer, 1991). The off-diagonal features are quite symmetrical with respect to the diagonals in both quadrants, and this agrees well with the theory (Shane et al., 1992; Höfer, 1994). Two pairs corresponding to the $\nu_{dq\pm}$ transitions of the $^{14}N(1)$ and $^{14}N(2)$ are clearly observed in the negative (+, −) quadrant of the plot. The pair at (+3.9, −7.6; +7.6, −3.7) MHz correlates with the double-quantum peaks at 3.86 and 7.41 MHz observed in the three-pulse ESEEM spectrum, and this observation confirms the assignment of the two frequencies in Figure 2A to $^{14}N(1)$. The two $\nu_{dq\pm}$ peaks at 4.71 and 8.8 MHz in Figure 2A that are assigned to $^{14}N(2)$ are also correlated in the contour plot where they appear as two cross-peaks at (+5.4, −9.3; +9.3, −5.2) MHz. The small difference between the position of the peaks in the one- and two-dimensional spectra may originate from differences in the data analysis that is used to obtain the Fourier transforms for each type of spectrum. For the two-dimensional spectra, no dead time reconstruction is performed contrary to the case with the one-dimensional spectra (see Materials and Methods), and this may lead to small shifts in the frequency positions in each type of experiment. Nevertheless, there is no doubt that the strong peaks observed in the negative quadrant in Figure 4 are correlation peaks of

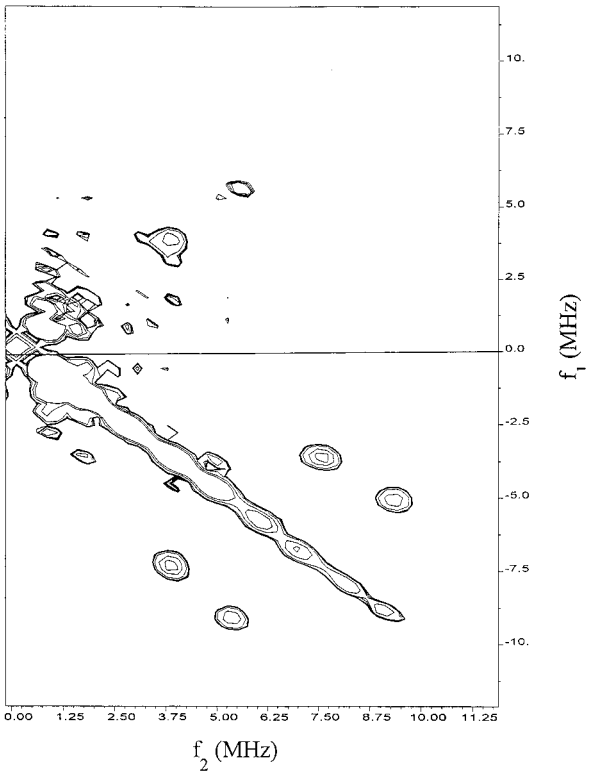

FIGURE 4: Contour plot of the HYSCORE experiment for VO^{2+} complexed with TF1 (0.9 VO^{2+}/TF1) after FT and magnitude calculation. Experimental conditions were the following: temperature, 4.2 K; microwave frequency, 9.57 GHz; $f_1f_2 = 200 \times 200$ points; starting values, $t_1 = t_2 = 80$ ns; time increments, $\Delta t_1 = \Delta t_2 = 8$ ns; $\tau = 456$ ns; $\pi/2$ pulse, 16 ns; π pulse, 40 ns; time interval between successive spin echo pulse sets, 7.7 ms; and magnetic field setting, 3415 G. The recorded data set was processed by a polynomial baseline correction and a Hamming apodization in t_1 and t_2 prior to zero filling and two-dimensional FT.

the two $\nu_{dq\pm}$ of the two ^{14}N coordinating the VO^{2+} in TF1. Correlation peaks between ν_{dq-} and ν_{dq+} have already been observed for VO^{2+} with ^{14}N ligands in inorganic complexes or proteins, in the negative quadrant (Shergill et al., 1995; Dikanov et al., 1995b) or in the positive quadrant (Reijerse et al., 1991; Shane et al., 1992). In addition, the features in the negative quadrant of Figure 4 have distinct elliptical shapes with the major axes parallel to the diagonal. This is because small anisotropic hyperfine interactions, which are also responsible for the line shape of the double-quantum transitions in the one-dimensional ESEEM spectum affect ν_{dq+} and ν_{dq-} in the same way (Shane et al., 1992; Höfer, 1994).

HYSCORE data were also recorded for samples of VO^{2+} bound to imidazole and VO^{2+} bound to glycine, both at a magnetic field corresponding to the central line of the EPR spectrum (not shown). At $\tau = 256$ ns, the data for imidazole were quite similar to those published by Dikanov et al. (1995b), with characteristic cross-peaks at (+4.9, −8.9; +8.9, −5.0) MHz from the double-quantum transitions in the negative quadrant. Additional correlations between single-quantum transitions were also detected in both the negative and positive quadrants. Dikanov et al. (1995b) have shown that imidazole is a good model for coordination of VO^{2+} by the histidine side chain in proteins. Thus, the similarity between the HYSCORE data of VO^{2+} bound to imidazole and to TF1 is also interpreted as a similarity of the VO^{2+} coordination in both samples. The HYSCORE of VO^{2+}

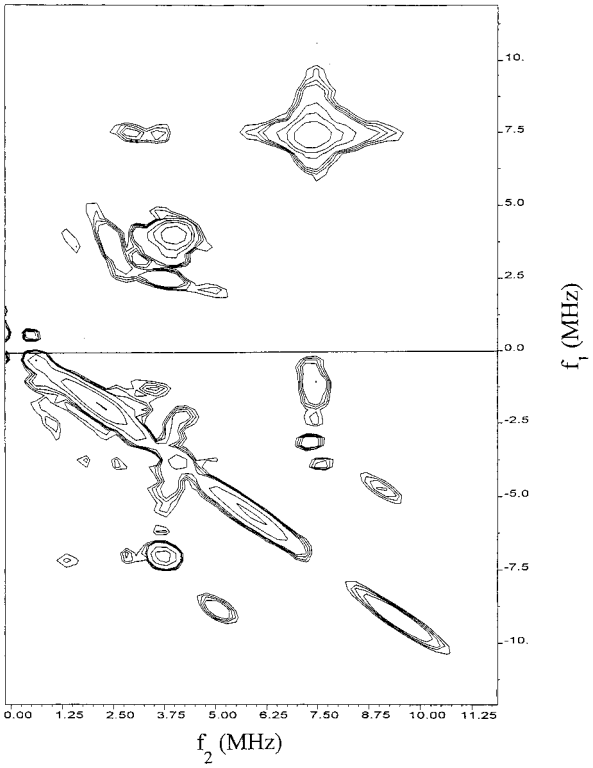

FIGURE 5: Contour plot of the HYSCORE experiment for VO^{2+} complexed with $\alpha_3\beta_3\gamma$ (0.4 $VO^{2+}/\alpha_3\beta_3\gamma$) after FT and magnitude calculation. Experimental conditions and data handling were the same as in Figure 4 except for the following: microwave frequency, 9.59 GHz; τ = 128 ns; π pulse, 32 ns; time interval between successive spin echo pulse sets, 30.7 ms; and a magnetic field setting, 3427 G.

complexed with glycine was also recorded with $\tau = 456$ ns, in order to avoid the suppression effect on the double-quantum cross-peaks (Höfer, 1994). Correlation peaks were manifest in the negative quadrant at (+3.75, −7.4; +7.5, −3.7) MHz, thereby also confirming the assignment of the corresponding three-pulse ESEEM peaks at 3.8 and 7.45 MHz to $\nu_{dq\pm}$ transitions from ^{14}N. These observations fully support a model in which VO^{2+} bound to TF1 in a ratio of 0.9/1 has at least two ^{14}N ligands: a first $^{14}N(1)$ belonging to the deprotonated amine of a lysine residue and a second $^{14}N(2)$ belonging to the imidazole ring of a histidine residue.

At least two additional pairs of cross-peaks are also visible in the positive quadrant (+, +) in Figure 4; these are perfectly symmetrical at (1.7, 3.8) and (0.7, 2.7) MHz. The (1.7, 3.8) pair probably reflects the correlation between the ν_{dq-} of $^{14}N(1)$ at 3.8 MHz and one of the single-quantum transition from the $M_S = +^1/_2$ of the same $^{14}N(1)$ at ≈1.7 MHz. The other pair at (0.7, 2.7) MHz probably arises from the correlation between two single-quantum peaks (one in each manifold) from either $^{14}N(1)$ or $^{14}N(2)$. Correlations between single-quantum transitions have also been described for VO^{2+} complexed with methylimidazole (Reijerse et al., 1991; Shane et al., 1992).

Figure 5 shows the HYSCORE contour plot of VO^{2+} bound to the $\alpha_3\beta_3\gamma$ complex in a ratio of 0.4/1. There again, cross-peaks that correlate with the double-quantum transitions identified in the one dimensional spectrum are clearly seen in the negative quadrant at (+3.7, −7.1; +7.1, −3.4) and (+4.9, −8.8; +8.8, −4.9) MHz. These are assigned to the $^{14}N(1)$ and $^{14}N(2)$ nitrogens, respectively. It is striking to note that the pair at (+4.9, −8.8) MHz from $^{14}N(2)$ in the HYSCORE contour plot is so well resolved, although the corresponding one dimensional frequency peaks appeared to be much smaller at ≈4.6 and 8.6 MHz, also compared with that of $^{14}N(2)$ in the TF1 ESEEM spectrum at 4.71 and 8.8 MHz (Figure 2). This probably reflects the increased resolution of the HYSCORE technique, in particular in its potential to discriminate frequency peaks that overlap in the one dimensional ESEEM spectrum (Höfer, 1986; Shane et al., 1992).

Interaction of the added nucleotide ATP with Mn^{2+} bound at the M1 site in TF1 has recently been demonstrated (Buy et al., 1996). A hyperfine coupling constant $|A| \approx 4.5$ MHz between Mn^{2+} and ^{31}P was inferred from the ESEEM spectra, which was taken as evidence for binding of one of the ATP phosphates to the Mn^{2+}. In addition, a significant increase in the hyperfine coupling to $|A| \approx 5.1$ MHz was detected after a period of incubation of the enzyme, which was interpreted as a conformational change involving the $Mn\cdots P_i$ bond(s). To test and refine the interpretation of this effect with VO^{2+} bound to the M1 site of TF1, and to potentially use the HYSCORE technique to discriminate between the hyperfine couplings with the different phosphate groups of the nucleotide ligand, ternary complexes with TF1, VO^{2+}, and ATP were studied by ESEEM and HYSCORE. As mentioned above, the EPR spectrum of VO^{2+} bound to TF1 supplemented with VO^{2+} and ATP (3 ATP/VO^{2+}) in a ratio of 0.93 VO^{2+}/protein is characterized by magnetic parameters that are different from those obtained for TF1 with only VO^{2+} added, indicating that VO^{2+} binds to ATP (see Table 2). The three-pulse ESEEM spectrum of this TF1·VO·ATP sample showed four strong peaks attributed to the interaction of VO^{2+} with $^{14}N(1)$ and $^{14}N(2)$, as well as the peak of the weakly coupled protons, just like the complex with no ATP (not shown). However, a new peak appeared in the ESEEM spectrum at ≈1.3 MHz, but that was difficult to characterize due to overlap with the Fourier transform of the unmodulated decay function. Figure 6 shows the contour plot of the HYSCORE data recorded for this complex. As expected, strong correlations at (+8.8, −5.0; +4.9, −8.9) MHz connect the double-quantum transitions of $^{14}N(2)$; it is also of note that the corresponding correlations for $^{14}N(1)$ are absent in the negative quadrant, and this effect is probably due to the choice of $\tau = 128$ ns (instead of $\tau = 456$ ns for the spectra in Figure 4) which induces a suppression effect for these frequencies (Höfer, 1994). It was verified that the expected correlations were observed at the correct frequencies when using other τ values (not shown). In addition, two additional main new pairs of correlations are detected for the TF1·VO·ATP sample at (+1.7, +10.5; +10.6, +1.9) and (+2.1, −13.4; +13.5, −2.0) MHz. The first pair could correlate the peak at ≈1.3 MHz detected in the one-dimensional spectrum with another frequency at ≈10.55 MHz that remained undetected in the one-dimensional ESEEM. To refine the assignment of the HYSCORE correlations in Figure 6, data were also recorded for VO^{2+} complexed with ATP, in an attempt to extract the hyperfine coupling parameters with ^{31}P from phosphates bound to VO^{2+}.

Two correlation pairs can be identified in the HYSCORE plot displayed in Figure 7: the first in the positive quadrant at (+1.5, +10.5; +10.5, +1.5) MHz and the second in the negative quadrant at (+1.5, −13.2; +13.2, −1.5) MHz. Apart from the protons, the only other type of nucleus in the ATP ligand with significant abundance and non-zero nuclear spin

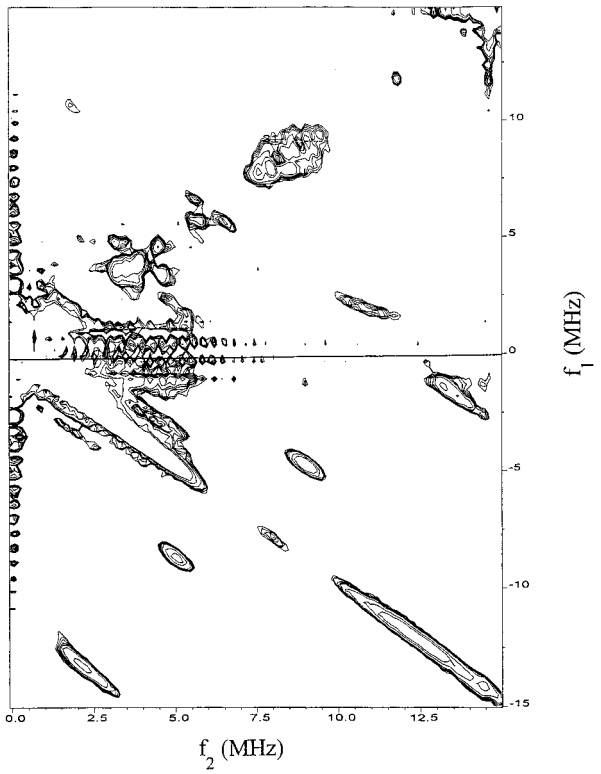

FIGURE 6: Contour plot of the HYSCORE experiment for the VO•-TF1•ATP complex (0.93 VO^{2+}/TF1 and 3 ATP/VO^{2+}) after FT and magnitude calculation. Experimental conditions and data handling were the same as in Figure 4 except for $\tau = 128$ ns and a magnetic field setting of 3419 G.

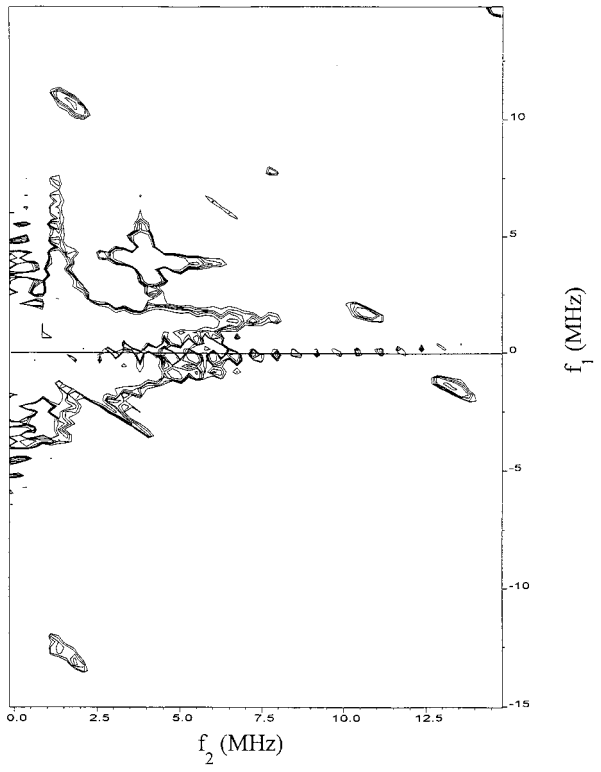

FIGURE 7: Contour plot of the HYSCORE experiment for VO^{2+} with ATP in maleic acid at pH 6.3 after FT and magnitude calculation. Experimental conditions and data handling were the same as in Figure 4 except for a microwave frequency of 9.69 GHz, $\tau = 128$ ns, and a magnetic field setting of 3462 G.

is ^{31}P ($I = {}^1/_2$). Thus, the observed features can only originate from ^{31}P nuclear frequencies. For a spin system with $S = {}^1/_2$ and $I = {}^1/_2$, in the case of weak hyperfine anisotropy, the modulation frequencies in the stimulated ESEEM can be approximated by (Dikanov & Tsvetkov, 1992)

$$\nu_{a,b} = |\nu_L \pm {}^1/_2 A_{zz}| \quad (3)$$

where the $\nu_{a,b}$ values are the two nuclear transition frequencies associated with the two electron spin states $M_S = \pm {}^1/_2$, ν_L is the Larmor frequency of the nucleus with $I = {}^1/_2$, and A_{zz} is the projection of the hyperfine tensor onto the z direction of the electron spin operator. If $|A_{zz}| < 2\nu_L$, the two frequencies are within the frequency range $0-2\nu_L$ and the HYSCORE correlation features will appear in the positive quadrant as a pair of cross-peaks at (ν_a, ν_b) and (ν_b, ν_a) (Höfer, 1994). When $|A_{zz}| > 2\nu_L$, ($\nu_L - {}^1/_2 A_{zz}$) < 0 and ($\nu_L + {}^1/_2 A_{zz}$) > $2\nu_L$; the HYSCORE correlations will then appear in the negative quadrant as a pair of cross-peaks at (ν_a, $-\nu_b$) and (ν_b, $-\nu_a$). For a spin system in a powder pattern which is the case in the present study, the correlation peaks may become ridges due to hyperfine anisotropy; these ridges run approximately perpendicular to the diagonal in the positive quadrant and parallel to the diagonal in the negative quadrant (Shane et al., 1992; Höfer, 1994).

The two pairs of cross-peaks in Figure 7 for the VO^{2+} complex with ATP can be interpreted according to this theory. The ridges in the positive quadrant are perpendicular to the diagonal, and they are centered at (+1.5, +10.5; +10.5, +1.5) MHz and have their middle point on the diagonal at (+6.0, +6.0) MHz. This latter value fits well with the Larmor frequency of ^{31}P ($\nu_L = 5.97$ MHz in the experimental conditions), and therefore, the corresponding features are assigned to coupling with a first ^{31}P nucleus, $^{31}P(a)$, with $A_{zz}(a) \approx 9 \pm 1$ MHz. This clearly fulfills the condition $|A_{zz}| < 2\nu_L$, as expected from the observation of the ridges in the positive quadrant (Höfer, 1994). In addition, the data confirm that the hyperfine interaction with ^{31}P is mainly isotropic with a weak anisotropic part that is illustrated by the distribution in the values of $A_{zz}(a)$ (Höfer, 1994). This in turn indicates that the detected ^{31}P originates from a phosphate group that coordinates the VO^{2+}. In the negative quadrant in Figure 7, ridges parallel to the diagonal are identified which are centered at (+1.5, −13.2; +13.2, −1.5) MHz, corresponding to a distance in coordinates of ≈11.7 MHz. This is roughly twice the Larmor frequency of ^{31}P, and the ridges are therefore assigned to coupling with a second ^{31}P nucleus, $^{31}P(b)$. A line joining the centers of the ridges would cross the diagonal at (+7.4, −7.4) MHz, leading to $A_{zz}(b) = 14.8$ MHz, with a distribution of ±1.2 MHz which is estimated from the edges of the ridges. This again fulfills the condition $|A_{zz}| > 2\nu_L$, as expected for HYSCORE features in the negative quadrant (Höfer, 1994). It is of particular note that the two pairs identified here certainly do not arise from the interaction of VO^{2+} with the same ^{31}P nucleus; when the anisotropy of the hyperfine interaction is not negligible, the correlation ridges appear like arcs, or horns in the case of rhombic interaction, that run perpendicular or parallel to the diagonal depending on the relative size of A_{zz}. These ridges are expected to spread over the whole range of hyperfine couplings (Reijerse & Dikanov, 1992; Höfer, 1994; Dikanov & Bowman, 1995). In this respect, the patterns of ridges in Figure 7 do appear like portions of arcs whose centers are given above, and the

Table 4: Hyperfine Coupling Parameters for ^{31}P in Complexes with VO^{2+} Estimated from the HYSCORE Data

complexing ligand	$A_\perp$ (MHz)	$A_\parallel$ (MHz)	assignment
ATP and maleate (pH 6.7)	13.6	16.0	$^{31}P_\beta$
	8.0	10.0	$^{31}P_\gamma$
ATP and TF1	14.3	16.7	$^{31}P_\beta$
(0.93 VO^{2+}/TF1 and 3 ATP/VO^{2+})	7.2	10.2	$^{31}P_\gamma$
ATP and $\alpha_3\beta_3\gamma$	14.2	15.8	$^{31}P_\beta$
(1.4 VO^{2+}/$\alpha_3\beta_3\gamma$ and 3 ATP/VO^{2+})	6.2	9.2	$^{31}P_\gamma$

distributions around the central values probably represent estimates of the anisotropic portions of hyperfine interactions with axial symmetry (Table 4).

The correlation features in Figure 6 are also interpreted within this framework. The ridges at (+1.7, +10.5; +10.6, +1.9) MHz are more or less perpendicular to the diagonal, and their middle point at (+6.15, +6.15) MHz roughly corresponds to the Larmor frequency of ^{31}P (5.90 MHz in the experimental conditions). The calculated $A_{zz}(a) = 8.7$ MHz originates from the interaction of a first phosphorus atom $^{31}P(a)$ with VO^{2+}, similar to the VO^{2+} complex with ATP. The correlation features in the negative quadrant at (+2.1, −13.4; +13.5, −2.0) MHz appear parallel to the diagonal and are separated by 11.4 MHz, which is roughly twice the ^{31}P Larmor frequency. They are assigned to coupling with a second $^{31}P(b)$ with $A_{zz}(b) = 15.5 \pm 1.2$ MHz. Both couplings are similar to those measured above for VO^{2+} with ATP. They are, however, somewhat but significantly smaller in magnitude than hyperfine couplings between VO^{2+} and ^{31}P that have been reported for metal sites in proteins. Couplings of 8.5 G (23.8 MHz) and 22 MHz have been measured by EPR in AdoMet synthetase (Markham, 1984; Markham & Leyh, 1987), and in CF1, coordination by phosphates from the ATP has been inferred from the hyperfine couplings $A_\perp = 18.5$ and 20 MHz measured by EPR for the M2 and M3 metal binding sites (Houseman et al., 1994b). The results reported here from HYSCORE data of $A_{zz} = 8.7$ and 15.5 MHz for two coupled ^{31}P with VO^{2+} indicate also a coordination by two phosphate groups for VO^{2+} in the M1 site, which probably add to the two nitrogen ligands from a lysine and a histidine residue from the protein.

When VO^{2+} and ATP (3 ATP/VO^{2+}) were added simultaneously to the $\alpha_3\beta_3\gamma$ complex in a stoichiometry of 1.4 VO/$\alpha_3\beta_3\gamma$, the three-pulse ESEEM spectrum at 3420 G showed no significant modulation except that from the weakly coupled protons at ≈14.55 MHz (not shown). In particular, the very intense and sharp peaks at 3.85 and 7.25 MHz arising from the $\nu_{dq\pm}$ of the lysine $^{14}N(1)$ could no longer be seen in the ESEEM. The HYSCORE data for this sample display no correlation peaks for this $^{14}N(1)$ either, but the features corresponding to the histidine $^{14}N(2)$ are present as a pair at (+5.0, −8.9; +9.0, −4.9) MHz (not shown). The fact that the corresponding $^{14}N(2)$ $\nu_{dq\pm}$ peaks are hard to detect in the one-dimensional ESEEM spectrum can be compared with the observations made above for the sample with VO^{2+} and $\alpha_3\beta_3\gamma$, for which the double-quantum transitions of $^{14}N(2)$ were far less intense than those of $^{14}N(1)$ (Figure 2B). The contour plot also shows the pairs at (+2.4, +10.7; +10.5, +2.0) and (+1.8, −13.2; +14.0, −1.8) MHz corresponding to the $^{31}P(a)$ and $^{31}P(b)$ couplings. These results indicate that the added VO^{2+} and ATP moieties [probably as $VO(ATP)_2$; see Mustafi et al. (1992)] really bind to the $\alpha_3\beta_3\gamma$ complex in the M1 site with the resulting VO^{2+} ligands including the histidine imidazole $^{14}N(2)$ and two phosphate groups from ATP. It is of particular note for the interpretation given here of the formation of a ternary complex between $\alpha_3\beta_3\gamma$, VO^{2+}, and ATP that the $\nu_{dq\pm}$ features of $^{14}N(1)$ are absent from both the one dimensional ESEEM and the HYSCORE data, indicating that the spectra cannot be interpreted as arising from the superposition of the individual spectra of $VO(ATP)_2$ and VO·TF1, were only these complexes present in the sample. This also probably strengthens the evidence for the formation of the ternary VO·TF1·ATP complex reported above.

DISCUSSION

The data from EPR, ESEEM, and HYSCORE reported in the present study for TF1 ATPase and the subcomplex $\alpha_3\beta_3\gamma$ in the presence of VO^{2+} and ATP provide evidence for binding of the VO^{2+} cation to a high-affinity metal binding site both in the presence and in the absence of ATP and for the formation of the ternary complexes VO·TF1·ATP and VO·$\alpha_3\beta_3\gamma$·ATP. This high-affinity metal binding site is probably similar to the M1 site that has been described in CF1 (Buy et al., 1996). Further, the analysis and simulations of the EPR spectra, together with the information obtained from the one-dimensional ESEEM and two-dimensional HYSCORE experiments, provide much new information on the protein ligands of VO^{2+} in the M1 site of TF1 and $\alpha_3\beta_3\gamma$ and the interaction with the substrate ATP.

When VO^{2+} is bound to TF1 in the absence of ATP, the spectroscopic data strongly suggest that two ^{14}N from the protein coordinate the VO^{2+} in the equatorial position. VO^{2+} complexes with glycine and imidazole were also studied as models for the VO^{2+} interaction with ^{14}N. As a result, the hyperfine couplings $A_{iso(1)} = 4.75$ MHz and $A_{iso(2)} = 6.5$ MHz measured for the VO·TF1 complex are attributed to couplings with two ^{14}N nuclei, namely from the terminal amine of a lysine and the imidazole ring of a histidine, respectively. The present interpretation is supported by ESEEM results already published in the literature, where VO^{2+} protein complexes with different equatorial nitrogen ligands have been characterized (Tipton et al., 1989; Gerfen et al., 1991; Zhang et al., 1993; Dikanov et al., 1995a; Fukui et al., 1995). From these studies, it appears that the A_{iso} values reported for the amino ^{14}N from a lysine residue coordinating the VO^{2+} in equatorial position are in the range of 4.3−5.2 MHz, whereas the couplings with the imine ^{14}N of the imidazole ring of a histidine are in the range of 6.0−7.6 MHz.

In a recent study, Buy et al. (1996) proposed that Mn^{2+} bound to the M1 site of TF1 is coordinated by the N_ϵ of deprotonated β-Lys-164.[3] This lysine residue is in fact highly conserved in the amino acid sequence of β subunits of ATPases from different organisms, as part of the "P-loop" consensus sequence of the catalytic site, and the corresponding β-Lys-178 in CF1 has been proposed to bind the divalent metal in the M3 site (Houseman et al., 1994a, 1995). In addition, the mutation of β-Lys-164 in TF1 to an isoleucine has been shown to induce a strong inhibitory effect on the ATPase activity of reassembled mixtures of the α, β, and γ subunits of TF1 (Yohda et al., 1988). In the F1 enzyme

[3] In the previous report (Buy et al., 1996), the amino acid numbering (β-Lys-162) was made according to the sequence of the β subunit of the analogous mitochondrial F1. The corresponding conserved lysine residue in TF1 is β-Lys-164 (Tozawa et al., 1993).

from *E. coli*, ATP synthesis and hydrolysis were strongly impaired in mutants of the β subunit in which the corresponding β-Lys-155 was changed to a glutamine or a glutamate, demonstrating that the lysine is a critical catalytic residue (Senior et al., 1993). The important roles that have been reported for this conserved lysine in the β subunit of F1 can probably be related to its binding to the divalent metal cation as suggested for β-Lys-164 in TF1 in the present and earlier studies.

The spectroscopic data also indicate that VO^{2+} is coordinated by the imino nitrogen of a histidine imidazole in the M1 site. This result is somewhat surprising because the ESEEM data of Mn^{2+} bound to this metal site did not show any evidence for such a histidine ligand (Buy et al., 1996). In addition, the ESEEM data that have been reported for the M2 and M3 sites are not interpreted in terms of a histidine ligand either (Houseman et al., 1994a, 1995; Buy et al., 1996). The following observations are, however, relevant to this question. From CW EPR data of the M2 and M3 metal binding sites in CF1, Houseman et al. (1994b, 1995) demonstrated that nucleotides do interact with VO^{2+}. Buy et al. (1996) also showed that Mn^{2+} in the M1 site of CF1 interacts with the strongly bound ADP, and analogous results were found with TF1 and exogenous ATP. These results demonstrated a close proximity between sites for metal binding and those for binding of nucleotides for at least three of these sites. In fact, the spectroscopic data reported above for the VO·TF1·ATP complex demonstrate that ATP interacts with VO^{2+} in the M1 site by binding through two phosphate groups. This also supports a model in which the M1 metal site in TF1 is close to a nucleotide binding site. The crystal structure of the homologous mitochondrial F1 (MF1) shows only one histidine residue in the environment of those nucleotide binding sites that are mainly positioned in the β subunits (Abrahams et al., 1994). This histidine residue, β-His-328, corresponds to β-His-324 in the *Bacillus* enzyme, as judged from the analyses of the amino acid sequences (Walker et al., 1985; Tozawa et al., 1993). In MF1, β-His-328 belongs to the last turn of the α helix G of the β subunit of MF1 (Abrahams et al., 1994). On the other hand, Michel et al. (1995) showed that one of the amino acids involved in binding azidophenyl [α-^{32}P]pyrophosphate, a pyrophosphate mimic, was β-Tyr-311, a residue that belongs to β sheet 7 of the β subunit of MF1, which is related by a loop to α helix G (Abrahams et al., 1994). To explain the photolabeling of β-Tyr-311 by the azido derivative, Michel et al. (1995) have suggested that the peptide segment encompassing this β-Tyr-311 is somewhat flexible. Similarly, α helix G could also present some flexibility in TF1, in a way that would allow binding of the nearby VO^{2+} in the M1 site by the imino ^{14}N of the β-His-324 side chain. This interpretation would then identify the histidine ligand detected here for the VO^{2+} in the M1 site as β-His-324 in the environment of the nucleotide binding site.

The oxovanadium cation VO^{2+} is made of V(IV) double bonded to an oxo ligand. The resulting V═O distances are very short and range from 1.55 to 1.68 Å depending on the ligand set, in particular the coordination *trans* to the oxo bond (Cotton & Wilkinson, 1988). This results in an increased ionic volume for the VO^{2+} compared to that for the spherical Mg^{2+} and Mn^{2+} cations with effective ionic radii of 0.72 and 0.83 Å, respectively. On the other hand, ATP hydrolysis by CF1 has been reported to be activated to the same extent by VO^{2+}, Ca^{2+}, and Mg^{2+} (Houseman et al., 1994a). Results from this laboratory with the TF1 enzyme indicate a significantly lower activity in the presence of VO^{2+} compared to that in the presence of Mg^{2+} and Mn^{2+} (Table 1). The apparent discrepancy may simply arise from differences in the CF1 and TF1 enzymes, but it is of particular note that, in the CF1 study, a strongly bound Mg^{2+} cation remained associated with the protein (Houseman et al., 1994a), which may perhaps explain the differences in the activities. Because the enzymatic activities with Mg^{2+} and Mn^{2+} are so similar, and because no histidine binding was observed for Mn^{2+} in the M1 site, the differences in the spectroscopic properties exhibited by Mn^{2+} and VO^{2+} in the M1 site may in fact reflect the differences in the activities promoted by these cations. The larger ionic volume of VO^{2+} certainly perturbs the topology of the M1 binding site in TF1 in such a way that the proximal β-His-324 is now in binding position with regard to the metal cation. This probably also perturbs the enzymatic properties of both TF1 and the $\alpha_3\beta_3\gamma$ complex, thereby suggesting that the conserved β-His-324 in TF1 is also of critical importance, perhaps in positioning the terminal γ-phosphate of the ATP molecule through hydrogen bonding. In this respect, it is of note that, in the sequence alignments of the α and β subunits of F1 ATPases, this conserved histidine in the β subunits does not correspond to a histidine residue in the α subunits but instead corresponds to an isoleucine, a residue that is not expected to have a critical role in positioning the nucleotide.

When VO^{2+} and ATP are added to TF1, a ternary complex VO·TF1·ATP does form. The two-dimensional HYSCORE data clearly show that two different ^{31}P interact with VO^{2+}. The two corresponding phosphate groups are proposed to be the β- and γ-phosphates of the ATP, with $A_{zz}(^{31}P_\beta) = 15.5$ MHz and $A_{zz}(^{31}P_\gamma) = 8.7$ MHz in the enzyme complex. This is based on the following evidence. First, on the basis of EPR spectrometric titrations of VO^{2+}, it has been shown that the stoichiometry of metal−ligand binding for ADP and ATP was 1/2; the $VO(ADP)_2$ complex was found to be coordinated through the α- and β-phosphate oxygens in equatorial positions, with equivalent hyperfine couplings from the four ^{31}P, with $A \approx 18.5$ MHz (Mustafi et al., 1992). However, for the complex $VO(ATP)_2$, the hyperfine couplings with the ^{31}P nuclei were not resolved in the EPR spectra, and this was attributed to the nonequivalence of the phosphorus atoms from the equatorial β- and γ-phosphate ligands with distinct couplings for each ^{31}P, thereby yielding a broad unresolved EPR line (Mustafi et al., 1992). The measurement of two different ^{31}P couplings, $A_{zz} = 14.8$ MHz and $A_{zz} = 9.0$ MHz, in the HYSCORE data of $VO(ATP)_2$ in Figure 7 is in line with this earlier conclusion and suggests that these can probably be assigned to the $^{31}P_\beta$ and $^{31}P_\gamma$ of ATP. And second, the HYSCORE data obtained with samples with VO^{2+} and ATP at pH 2.3 showed only the interaction with $A_{zz}(^{31}P) = 9.0$ MHz (not shown), thereby identifying the latter with $^{31}P_\gamma$ on the basis of the relative pKs of the protonatable groups in ATP. The ^{31}P hyperfine couplings for the ternary complex VO·TF1·ATP are also very similar to those measured for the $VO(ATP)_2$ complex, suggesting a similar mode of coordination for the ATP ligand in the VO·TF1·ATP complex, although other modes of coordinations, e.g. by the α- and β-phosphates of the ATP, and/or mixed axial/equatorial coordinations cannot be completely ruled out (see below). The data also indicate that

ATP is probably not hydrolyzed in the VO·TF1·ATP complex, since both terminal phosphates are probably detected as VO^{2+} ligands. In addition, the spectroscopic results show that the two nitrogen ligands from the lysine and the histidine in the VO·TF1 complex are also ligands of the metal in the presence of ATP. It is of note that the interaction with a phosphate group from ATP was also demonstrated with Mn^{2+} in the M1 site of TF1, although the identity of the bound phosphate and the coordination by the lysine remained unclear in the Mn·TF1 complex after addition of ATP (Buy et al., 1996).

Houseman et al. (1994b, 1995) have interpreted ESEEM data using VO^{2+} as a paramagnetic probe for the M2 and M3 sites in CF1 as evidence for coordination of one phosphate from ATP in the equatorial position. To our knowledge, the difference between equatorial and axial coordination of phosphate ligands in terms of hyperfine couplings with ^{31}P has not been documented. It is therefore difficult to ascertain whether the proposed β- and γ-phosphate ligands detected here in the VO·TF1·ATP complex both bind in the equatorial position or if one of them binds in the axial position. Certainly, detailed spectroscopic data for crystallographically characterized VO^{2+} complexes with phosphate ligands would be necessary. Yet, the ENDOR results from Mustafi et al. (1992) clearly demonstrate the absence of an axial ligand from the nucleotide in the VO-$(ATP)_2$ complex. The ^{31}P hyperfine couplings that are measured from HYSCORE for both $VO(ATP)_2$ and the ternary complex with TF1 are also of similar magnitude (Table 4) and therefore also argue for an equatorial coordination of the two phosphates in the VO·TF1·ATP complex. In addition, the spectroscopic studies reported by Atherton and Shackleton (1980) and Tyryshkin et al. (1993) for VO^{2+} with aqua ligands demonstrate that the isotropic hyperfine couplings with all but one equatorial protons are 10−100 times larger than those with the axial water protons. If this observation can be extrapolated to the couplings with ^{31}P, the results presented here would then also indicate that both phosphates are equatorial ligands of the VO^{2+} in the complex with TF1.

The ligand environment of VO^{2+} bound to $\alpha_3\beta_3\gamma$ in the VO·$\alpha_3\beta_3\gamma$ complex is very similar to that in the VO·TF1 complex, as judged from the ESEEM and HYSCORE results. The measured hyperfine couplings with ^{14}N are similar for both sites, suggesting that VO^{2+} is also coordinated by β-His-324 and β-Lys-164 in the $\alpha_3\beta_3\gamma$ subcomplex. This probably indicates that the $\alpha_3\beta_3\gamma$ complex is a good structural model for the study of the sites for the divalent metal ions in TF1. This is not surprising in view of the measured catalytic activity of the complex as compared with that of the wild type enzyme (Table 1). The situation is somewhat different in the presence of ATP. When the sample with the binary complex VO·$\alpha_3\beta_3\gamma$ was supplemented with ATP, no change was detected in the ESEEM compared with that of VO·$\alpha_3\beta_3\gamma$, probably indicating no change in the coordination of the VO^{2+}. Similar observations were made for the TF1 complex. However, when VO^{2+} and ATP are added simultaneously to the $\alpha_3\beta_3\gamma$ complex, the spectroscopic data are evidence for the formation of the ternary complex with coordination of the VO^{2+} by the histidine imidazole (probably β-His-324) and two phosphates from the ATP. This is based on the similarities of the measured hyperfine couplings with those measured for the VO·$\alpha_3\beta_3\gamma$ and the $VO(ATP)_2$ complexes. This indicates that the amine ligand from the β-Lys-164 is apparently lost in the complex with ATP. This contrasts with the situation in the ternary complex VO·TF1·ATP discussed above, where both the histidine and the lysine residues remained ligands of the VO^{2+}. The reason for this difference is not known but could lie in differences in the accessibility of the ATP molecule or of $VO(ATP)_2$ for the $\alpha_3\beta_3\gamma$ complex compared to that of isolated TF1. The different behavior in terms of the spectroscopic properties in the presence of VO^{2+} and ATP reported here for TF1 and $\alpha_3\beta_3\gamma$ may correspond to functional differences, perhaps related to the absence of the small δ and/or ϵ subunits, that would change the type of or the properties of the metal site that is being filled by the VO^{2+} cation. In this respect, it should be emphasized that, although the present work demonstrates the relevance of VO^{2+} in terms of a spectroscopic probe for the structure of the Mg^{2+} site M1 in TF1, and probably the other metal sites also, the apparent weaker reactivation of the ATPase activity should not be underestimated.

ACKNOWLEDGMENT

We are grateful to Ms. Nadège Koubbi and Anne-Laure Chaissé for their skillful assistance in the extraction and purification of TF1. We also thank Drs. Gérard Berger, Francis Haraux, and Clotilde Policar for very useful discussions, Drs. François André and Pierre Falson for performing the sequence alignments, and Dr. Paul Mathis for his valuable interest and support of this work.

REFERENCES

Abrahams, J. P., Leslie, A. G. W., Lutter, R., & Walker, J. E. (1994) *Nature 370*, 621−628.

Ashby, C. I. H., Cheng, C. P., & Brown, T. L. (1978) *J. Am. Chem. Soc. 100*, 6057−6063.

Astashkin, A. V., Dikanov, S. A., & Tsvetkov, Y. D. (1985) *J. Struct. Chem. 26*, 363−368.

Atherton, N. M., & Shackleton, J. F. (1980) *Mol. Phys. 6*, 1471−1485.

Bonvoisin, J., Blondin, G., Girerd, J. J., & Zimmermann, J. L. (1992) *Biophys. J. 61*, 1076−1086.

Bruist, M. F., & Hammes, G. G. (1981) *Biochemistry 20*, 6298−6305.

Buy, C., Girault, G., & Zimmermann, J. L. (1996) *Biochemistry 35*, 9880−9891.

Chasteen, N. D. (1981) in *Biological Magnetic Resonance* (Berliner, L. J., & Reuben, J., Eds.) Vol. 3, pp 53−119, Plenum Press, New York.

Cosgrove, S. A., & Singel, D. J. (1990) *J. Phys. Chem. 94*, 8393−8396.

Cotton, F. A., & Wilkinson, G. (1988) in *Advanced Inorganic Chemistry, 5th* ed., John Wiley & Sons, New York.

Cross, R. L. (1988) *J. Bioenerg. Biomembr. 20*, 395−406.

Dikanov, S. A., & Tsvetkov, Y. D. (1992) in *Electron Spin Echo Envelope Modulation (ESEEM) Spectroscopy*, CRC Press, Boca Raton, FL.

Dikanov, S. A., & Bowman, M. K. (1995) *J. Magn. Reson. A 116*, 125−128.

Dikanov, S. A., Tyryshkin, A. M., Hüttermann, J., Bogumil, R., & Witzel, H. (1995a) *J. Am. Chem. Soc. 117*, 4976−4986.

Dikanov, S. A., Samoilova, R. I., Smieja, J. A., & Bowman, M. K. (1995b) *J. Am. Chem. Soc. 117*, 10579−10580.

Eaton, S. S., & Eaton, G. R. (1990) in *Vanadium in Biological Systems* (Chasteen, N. D., Ed.) pp 199−222, Kluwer Publishers, Dordrecht, The Netherlands.

Eaton, S. S., Dubach, J., More, K. M., Eaton, G. R., Thurman, G., & Ambruso, D. R. (1989) *J. Biol. Chem. 264*, 4776−4781.

Espe, M. P., Hosler, J. P., Ferguson-Miller, S., Babcock, G. T., & McCracken, J. (1995) *Biochemistry 34*, 7593−7602.
Fauth, J. M., Schweiger, A., Braunschweiler, L., Forrer, J., & Ernst, R. R. (1986) *J. Magn. Reson. 66*, 74−85.
Flanagan, H. L., & Singel, D. J. (1987) *J. Chem. Phys. 87*, 5606−5616.
Flanagan, H. L., & Singel, D. J. (1988) *J. Chem. Phys. 89*, 2585−2586.
Fukui, K., Ohya-Nishiguchi, H., & Kamada, H. (1993) *J. Phys. Chem. 97*, 11858−11860.
Fukui, K., Ohya-Nishiguchi, H., Nakai, M., Sakurai, H., & Kamada, H. (1995) *FEBS Lett. 368*, 31−35.
Gemperle, G., Aebli, G., Schweiger, A., & Ernst, R. R. (1990) *J. Magn. Reson. 88*, 241−256.
Gerfen, G. J., Hanna, P. M., Chasteen, N. D., & Singel, D. J. (1991) *J. Am. Chem. Soc. 113*, 9513−9519.
Girault, G., Berger, G., Galmiche, J. M., & André, F. (1988) *J. Biol. Chem. 263*, 14690−14695.
Heaton, F. W. (1990) in *Metal Ions in Biological Systems* (Sigel, H., & Sigel, A., Eds.) Vol. 26, pp 119−133, Marcel Dekker, Inc., New York.
Hiller, R., & Carmeli, C. (1985) *J. Biol. Chem. 260*, 1614−1617.
Höfer, P. (1991) in *Electron Magnetic Resonance of Disordered Systems* (Yordanov, N. D., Ed.) pp 1−15, World Scientific, Singapore.
Höfer, P. (1994) *J. Magn. Reson. A 111*, 77−86.
Höfer, P., Grupp, A., Nebenführ, H., & Mehring, M. (1986) *Chem. Phys. Lett. 132*, 279−282.
Houseman, A. L. P., Morgan, L., LoBrutto, R., & Frasch, W. D. (1994a) *Biochemistry 33*, 4910−4917.
Houseman, A. L. P., LoBrutto, R., & Frasch, W. D. (1994b) *Biochemistry 33*, 10000−10006.
Houseman, A. L. P., LoBrutto, R., & Frasch, W. D. (1995) *Biochemistry 34*, 3277−3285.
Kevan, L. (1990) in *Modern Pulsed and Continuous-Wave Electron Spin Resonance* (Kevan, L., & Bowman, M. K., Eds.) pp 231−266, Wiley Interscience, New York.
Larsen, R. G., Halkides, C. J., & Singel, D. J. (1993) *J. Chem. Phys. 98*, 6704−6721.
Lucken, E. A. C. (1969) in *Nuclear Quadrupole Coupling Constants*, pp 217−248, Academic Press, London and New York.
Markham, G. D. (1984) *Biochemistry 23*, 470−478.
Markham, G. D., & Leyh, T. S. (1987) *J. Am. Chem. Soc. 109*, 599−600.
Matsui, T., & Yoshida, M. (1995) *Biochim. Biophys. Acta 1231*, 139−146.
Michel, L., Garin, J., Vinçon, M., Gagnon, J., & Vignais, P. (1995) *Biochim. Biophys. Acta 1228*, 67−72.
Mims, W. B., & Peisach, J. (1981) in *Biological Magnetic Resonance* (Berliner, L. J., & Reuben, J., Eds.) Vol. 3, pp 213−263, Plenum Press, New York.
Mulks, C. F., Kirste, B., & van Willigen, H. (1982) *J. Am. Chem. Soc. 104*, 5906−5911.
Mustafi, D., Telser, J., & Makinen, M. W. (1992) *J. Am. Chem. Soc. 114*, 6219−6226.
Ohta, S., Yohda, M., Ishizuka, M., Hirata, H., Hamamoto, T., Otawara-Hamamoto, Y., Matsuda, K., & Kagawa, Y. (1988) *Biochim. Biophys. Acta 933*, 141−155.
Reijerse, E. J., & Dikanov, S. A. (1992) *Pure Appl. Chem. 64*, 789−797.
Reijerse, E. J., Shane, J., de Boer, E., Höfer, P., & Collison, D. (1991) in *Electron Magnetic Resonance of Disordered Systems* (Yordanov, N. D., Ed.) pp 253−271, World Scientific, Singapore.
Senior, A. E., Wilkes-Mounts, S., & Al-Shawi, M. K. (1993) *J. Biol. Chem. 268*, 6989−6994.
Shane, J. J., Höfer, P., Reijerse, E. J., & de Boer, E. (1992) *J. Magn. Reson. 99*, 596−604.
Shergill, J. K., Joannou, C. L., Mason, J. R., & Cammack, R. (1995) *Biochemistry 34*, 16533−16542.
Tipton, P. A., McCracken, J., Cornelius, J. B., & Peisach, J. (1989) *Biochemistry 28*, 5720−5728.
Tozawa, K., Miyauchi, M., & Yoshida, M. (1993) *J. Biol. Chem. 268*, 19044−19054.
Tyryshkin, A. M., Dikanov, S. A., & Goldfarb, D. (1993) *J. Magn. Reson. A 105*, 271−283.
Walker, J. E., Fearnley, I. M., Gay, N. J., Gibson, B. W., Northrop, F. D., Powell, S. J., Runswick, M. J., Saraste, M., & Tybulewicz, V. L. J. (1985) *J. Mol. Biol. 184*, 677−701.
Yohda, M., Ohta, S., Hisabori, T., & Kagawa, Y. (1988) *Biochim. Biophys. Acta 933*, 156−164.
Zhang, C., Markham, G. D., & LoBrutto, R. (1993) *Biochemistry 32*, 9866−9873.

BI961811B